ВЫСОКОМОЛЕКУЛЯРНЫЕ СОЕДИНЕНИЯ, Серия А, 2011, том 53, № 5, с. 704–709

ПРИРОДНЫЕ ПОЛИМЕРЫ

УДК 541.64:542.954:547.491.6

PREPARATION AND CHARACTERIZATION OF ELECTROSPUN SILK FIBROIN NANOFIBER WITH ADDITION OF 1-ETHYL-3-(3-DIMETHYLAMINOPROPYL) CARBODIIMIDE[1]

© 2011 г. Feng Zhang[a, b], Huan X. Zhang[b], Bao Q. Zuo[a, c], and Xue G. Zhang[b]

[a] College of Textile and Clothing Engineering, Soochow University, Ganjiang Eastern Road, Suzhou Jiangsu 215021, China

[b] Institute of Medical Biotechnology; Soochow University; Jiangsu Province Key Laboratory of Stem Cell; Soochow University, Suzhou Jiangsu 215007, China

[c] National Engineering Laboratory for Modern Silk, Soochow University, Renai Road, Suzhou Industrial Park, Suzhou Jiangsu 215123, China

e-mail: hzhang@suda.edu.cn, bqzuo@suda.edu.cn

Received October 1, 2010
Revised Manuscript Received January 12, 2011

Abstract—The silk fibroin (SF) nanofiber mats with good water resistance and mechanical property were directly prepared by adding crosslinker 1-Ethyl-3-(3-dimethylaminopropyl)-carbodiimide (EDC) into the electrospin solution. The effect of EDC on the morphology, structure and physical properties of SF nanofiber mats was analyzed. With the addition of EDC, the average fiber diameter increased from 262 to 635 nm. The results from FTIR, TG-DTA and X-ray diffraction showed that EDC induced the structural transition from random coil to β-sheet conformation. Furthermore, the solubility and mechanical properties of SF nanofiber mats were obviously improved when the crosslinker EDC was used.

INTRODUCTION

Recently, many researchers have been interested in silk fibroin because of its outstanding mechanical properties, good biocompatibility, biodegradability and minimal inflammatory reaction [1–3]. To meet the demands of different applications, the native silk have been processed into different shapes, such as film [4], nanofiber mats [5], foams [6] and tubes [7]. However, the regenerated silk fibroin is water-soluble and has poor mechanical properties for their secondary structure is mainly random coil or α-helix conformation. The most common method to convert the random coil or α-helix conformation of silk fibroin into β-sheet conformation is to treat the SF by organic solvent, such as methanol or ethanol [8, 9]. With the methanol or ethanol post-treatment, the silk fibroin is water insoluble but very fragile with poor mechanical properties, especially under the wet conditions.

EDC is extensively used for its low toxicity, such as a crosslinker of collagen, hyaluronic acid, gelatin to improve their strength and stability [10, 11], covalently couple proteins to biomaterials, for example, couple recombinant human bone morphogenetic protein onto silk fibroin films [12], crosslink collagen with glycosaminoglycan [13], and immobilize Vascular Endothelial Growth Factor to the collagen scaffold [14].

In this paper, the SF nanofiber mats prepared by adding EDC into the electrospin SF-formic acid solution demonstrated good water resistance and mechanical property, and the effect of EDC crosslinker on the morphology, water stability, mechanical properties and secondary structure was investigated.

MATERIALS AND METHODS

Preparation of SF Nanofiber Mats

Raw *Bombyx mori* silk fibers were degummed three times with 0.5% (w/w) Na_2CO_3 solution for 30 min at 100°C, and then rinsed with distilled water. The degummed silk fibroin (SF) was dissolved in a mixture of solvents composed of LiBr/ethanol (40/60) for 6 h at 80°C. After a dialysis with a cellulose tubular membrane (molecular cutoff = 8000~14000, Sigma, USA) in distilled water for 3 days, the SF solution was filtered and then air-dried to obtain the regenerated SF films.

EDC (Shanghai Medpep Co. Ltd., Shanghai, China) was directly added into the 9% SF-formic acid solution (low speed stir for 1 h) that was prepared by dissolving regenerated SF films in 98% formic acid for 3 h (the weight ratio of EDC/SF was 1/9).

The electrospinning setup used in this study consists of a syringe and a needle (0.9 mm OD × 0.5 mm ID), a rectangular (20 × 10 cm) aluminum foil collecting plate, a high voltage power supply (which can supply positive voltage from 0 to 30 kV) (DW-P503-4AC, Dongwen High Voltage Power Tianjin Power Supply Plant, China), and a syringe pump (WZ-50C66T, Medical Instrument Corporation of Zhejiang University, Zhejiang, China). In the electrospinning process,

[1] Статья печатается в представленном авторами виде.

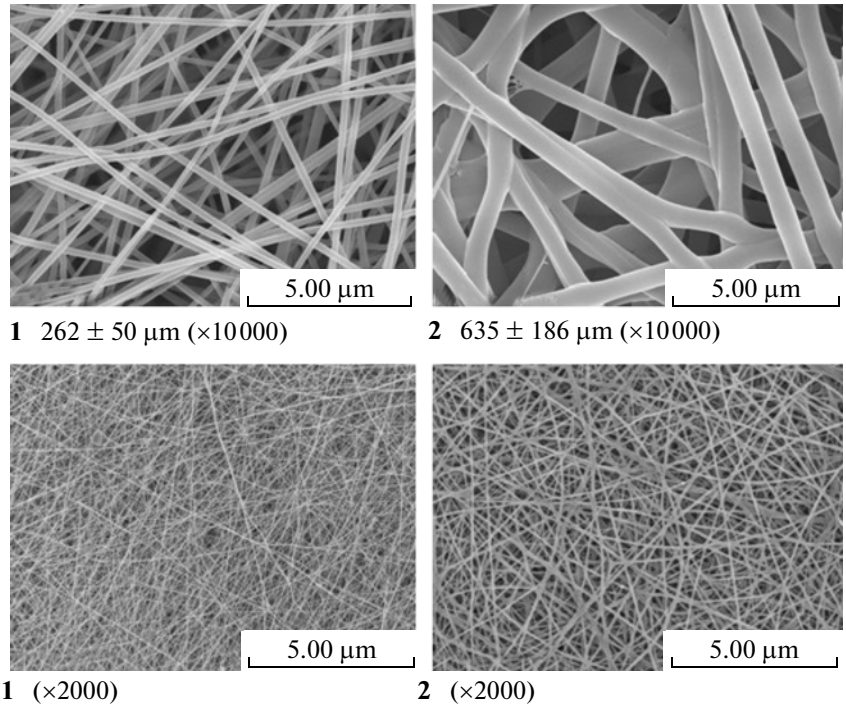

Fig. 1. SEM micrograph of SF nanofiber mats (**1** – non-crosslinked SF mats; **2** – crosslinked SF mats).

a high voltage of 12 kV was applied to the syringe needle, and then the electrospun SF nanofiber mats were collected on the collecting plate that was placed at a distance of 10 cm from the needle. Mass flow rate of solutions was 0.2 ml/h. The samples 1 and 2 are corresponding to non-crosslinked and crosslinked SF nanofiber mats, respectively. The electrospinning experiments were performed at room temperature.

Characterizing Techniques

Scanning electron microscopy. Before the diameter measurements of the nanofibers acquired randomly from SEM images using German Leica BME biomacroscope, the samples were mounted on copper plate and sputter-coated with 20–30 nm gold layer. For each sample, the diameter was the average of 100 measurements.

FTIR analysis. Fourier transform infrared (FTIR) spectra was obtained using a Magna spectrometer (NicoLET5700, America) in the spectral region of 400–4000 cm^{-1}. The powdered electrospun SF was pressed into potassium bromide (KBr) pellets prior to data collection.

X-ray diffraction analysis. The theta-theta diffractometer (X'PERT PRO MPD, PANalytical Company, Holland) with CuK_α radiation working at 40 kV and 40 mA was used to record X-ray diffractogram in the interval $2\theta = 20°–45°$ with scan rate 2 K/min.

TG-DTA analysis. Thermogravimetry/differential thermal analyses were performed with TG-DTA and PE-SII units (USA), between 40 and 380°C at a heating rate 10°C/min and nitrogen flow of 30 ml/min, the samples weight was about 5 mg.

Hot-water solubility test. The solubility of sample 1 and 2 in distilled water was evaluated at concentration of 1 mg/ml, and oscillated at 37.5°C water bath for 24 h. The water solubility was calculated using the average of 3 specimens coming from sample 1 and 2 with the following equation.

$$\text{Water solubility } (\%) = \frac{W_0 - W_1}{W_0} \times 100$$

W_0 is dry weight before hot water dissolution; W_1 is dry weight after hot water dissolution.

Tensile testing. Mechanical properties of samples 1 and 2 were determined by an automatic Tensile tester (Instron electronic strength tester 3365) at 20°C, and 65% RH. Strips measuring 5 × 0.5 cm were glued on a paper frame and then mounted on Instron tensile tester, and average tensile properties from five specimens were measured. The sample was broken by elongation rate 0.2 mm/s.

RESULTS AND DISCUSSION

Morphology of Electrospun SF Nanofiber Mats

Figure 1 shows SEM micrographs of the SF nanofiber mats electrospun with and without EDC (×2000 and 10000). The average diameter of a sample 1 (262 nm) was smaller than that of a sample 2 (635 nm). Also, the crosslinked fibers were not as

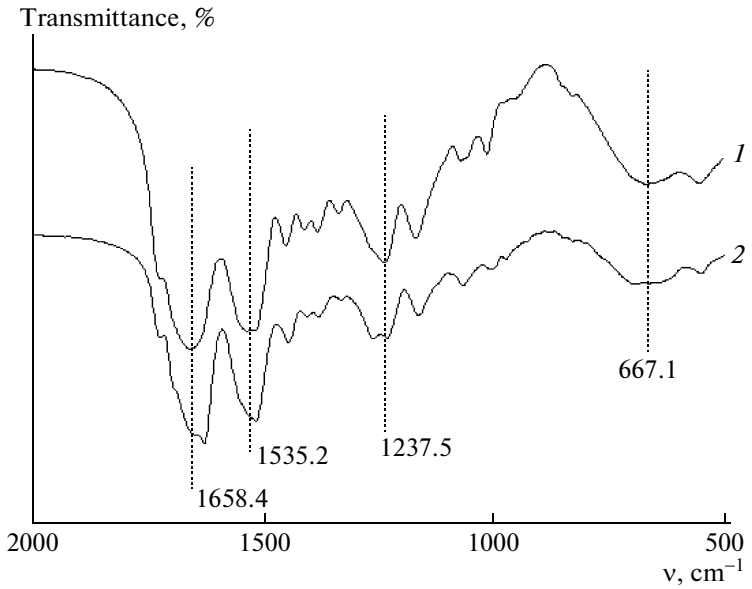

Fig. 2. FTIR spectra of SF nanofiber mats (*1* – non-crosslinked SF mats; *2* – crosslinked SF mats).

smooth in appearance as non-crosslinked ones. Compared with the non-crosslinked fibers, the surface of the crosslinked ones was much grainier and rougher, and the adhesion was significant.

FTIR

IR is a powerful and common tool for the protein conformations analysis, and is frequently used to investigate the conformation changes of silk fibroin [15]. Changes in structure of silk-fibroin nanofiber mats crosslinked by EDC were determined by FTIR, as shown in Fig. 2. There was no novel peak in sample 2, but the two samples exhibited completely different characteristic peaks which implied their different secondary structure. The absorption bands of sample 1 at wave number of 1658 cm^{-1} (amide I), 1535 cm^{-1} (amide II), 1237 cm^{-1} (amide III) and 667 cm^{-1} (amide IV) attributed to the random coil or α-helix conformation. These IR results suggested the prevailing amorphous structure of SF nanofiber mats electrospun without EDC. The FTIR absorbance peaks of sample 2 at 1631, 1520, and 696 cm^{-1} were generally considered to be characteristic of β-sheet structure. And the doublets at 1263 and 1237 cm^{-1} are assigned to amide III, and the signal at 1237 and 1263 cm^{-1} were associated with random-coil conformation and β-sheet conformation [5, 7], respectively.

Table 1. A content of secondary structures in electrospun SF nanofiber mats in per cents

Sample	β-sheet	Random coil	α-helix	β-turn
1	36.3248	19.2148	17.4649	26.9955
2	51.4649	8.8132	18.4683	21.2536

The secondary structure of silk fibroin could be analyzed quantitatively through an established technique which had been reported previously [16, 17]. Amide I absorption (1700–1600 cm^{-1}) was the most useful for determining protein secondary structures because it arised predominantly from C=O stretching vibration. It was well known that natural protein contains more than one secondary structure, so absorption peaks overlap in the amide I region to yield a featureless band, which had been resolved into several distinct bands by second-derivative. To determine the proportion of individual resolved amide I components, we interatively fitted Gaussian curves to deconvolved spectra. We assigned each separated amide I components to secondary structure based on previous studies [16, 17]. Table 1 shows the proportion of each secondary structure of electrospun nanofiber mats. Compared to sample 1, sample 2 had more abundant β-sheet and lower proportion of random coil and β-turn, and almost the same proportion of α-helix, which indicated that EDC induced the formation of β-sheet mainly from random coil.

X-ray Diffraction

X-ray diffraction was carried out to study the crystalline structure of the SF nanofiber mats. Figure 3 shows the diffraction pattern of the SF nanofiber mats. The non-crosslinked SF nanofiber (curve *1*) exhibited only one main diffraction peak at 22.4° corresponding to the spacing of 3.96 Å, attributed to Silk I. The crosslinked SF nanofiber (curve *2*) showed diffraction peaks at 20.8° and 23.8° corresponding to the spacing

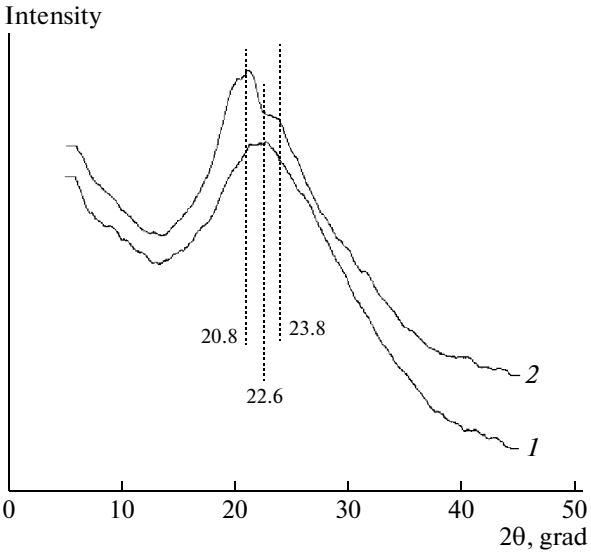

Fig. 3. X-ray diffraction of SF nanofiber mats (*1* – non-crosslinked SF mats; *2* – crosslinked SF mats).

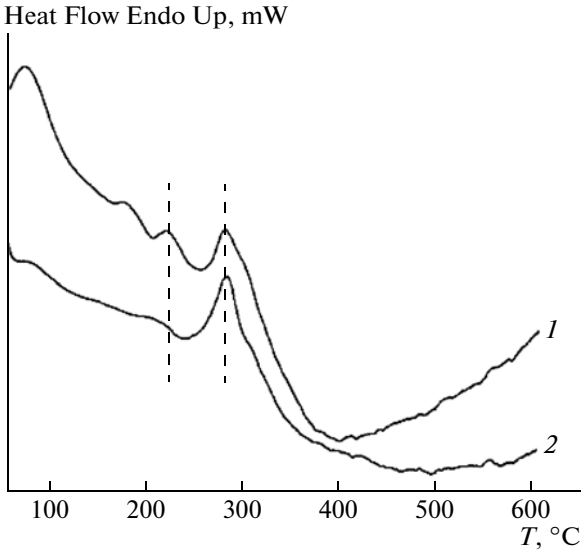

Fig. 4. DTA curve of SF nanofiber mats (*1* – non-crosslinked SF mats; *2* – crosslinked SF mats).

of 4.31, 3.70 Å, respectively, that were attributed to Silk II [18]. The main diffraction peak shifted from 22.4° to 20.6° and the new diffraction peak at 24.0° demonstrated that EDC crosslinker increased the formation of β-sheet structure from random coil. The results of X-ray diffraction were in accord with the FTIR analysis.

TG-DTA Curve

DTA curves were measured in order to investigate the thermal behavior of SF nanofiber mats. Figure 4 shows DTA-thermograms of SF nanofiber mats electrospun with or without EDC. The DTA curve of sample 1 showed a main endothermic peak at around 282°C which was attributed to the thermal decomposition of silk fibroin [19], and a endothermic peak at around 181°C which was the glass transition of SF, and a exothermic peak at around 207°C which was due to the structure transition from random-coil to β-sheet conformation [19]. When EDC was added into the electrospin solution, the corresponding SF mats (sample 2) demonstrated a higher main endothermic peak at 285°C, while the glass transition peaks and structural transition peak were hard to detect. Furthermore, the two curves all showed an obvious endothermic peak at about 224°C.

Figure 5 shows the differential thermogravimetric (DTG) curves of SF nanofiber mats. The tested samples showed two distinct negative peaks under the tested temperature: (*1*) small peak at 150–250°C; (*2*) major peak at 250–400°C. The DTG peaks represented specific thermal decomposition process accompanying weight loss.

The thermal decomposition temperature of silk fiber is about 320°C, which is detected in the case of well-oriented fiber containing β-sheet structure [20]. It suggested that the silk fibroin molecule of crosslinked SF nanofiber mats was oriented to some extent. From the DTG curves, we know that the endothermic peak at about 224°C in DTA curves because of a small weight loss. The TG-DTA analysis confirmed IR and X-ray diffraction results that structural transition of SF nanofiber mats from random coil to β-sheet structure.

Hot Water-Solubility

Water resistance of SF nanofiber mats was very important for biomedical application. Non-treated SF

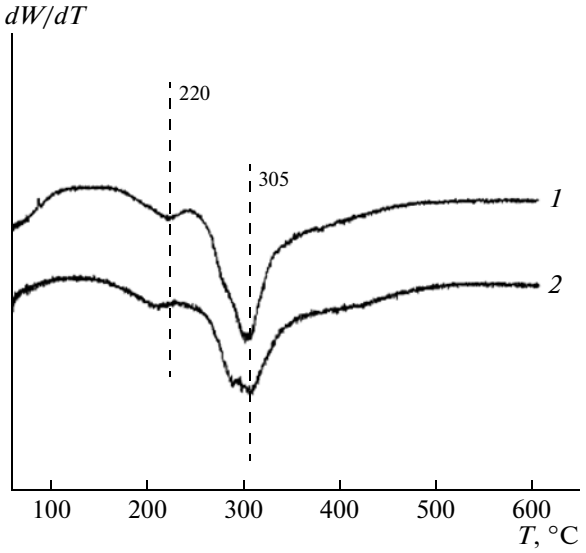

Fig. 5. DTG curve of SF nanofiber mats (*1* – non-crosslinked SF mats; *2* – crosslinked SF mats).

Table 2. Water solubility of SF nanofiber mats (1 – non-crosslinked SF mats; 2 – crosslinked SF mats)

Sample		Dry weight before dissolution	Dry weight after dissolution	Water solubility, %	Average, %
1	1'	0.0206	0.0135	34.61	36.4 ± 3.1
	2'	0.048	0.034	29.05	
	3'	0.044	0.028	36.36	
2	1'	0.0306	0.0253	17.37	16.6 ± 0.7
	2'	0.0214	0.0178	16.74	
	3'	0.0319	0.0269	15.67	

nanofiber mats were easily swollen and readily soluble in water. Usually, the SF nanofiber matrices were treated either with organic solution or with water vapor to enhance the stability of the nanofiber mats in water; however, these post-treated SF nanofiber mats were often very brittle. In our study, we added crosslinker EDC into electrospin solution to prepare water-resistance SF nanofiber mats whose weight loss was about 16% (as shown in Table 2), which was quite similar to that of mats treated with an aqueous methanol solution or water vapor. The weight loss of non-crosslinked SF nanofiber mats was about 36%, which was also similar to obtained in the previous report [21]. It is evident that the addition of EDC was highly effective in improving the water resistance, which made the water solubility to decrease from 36.4 to 16.6%.

Mechanical Properties

The mechanical property of SF nanofiber mats were tested, as shown in Table 3. The tensile strength of the crosslinked SF nanofiber mats was increased, compared to non-crosslinked SF nanofiber mats, mainly due to the increase of the crystalline regions and the EDC-crosslinke influence (like hydrogen bond) and fibers sintering (Fig. 1). Furthermore, the elongation at break of the crosslinked sample was substantially increased, indicating a network structure was formed due to the formation of the direct amide link within the silk fibroin. So, the increase of tensile strength and elongation at break made the SF nanofiber mats more suitable for practical tissue engineering applications.

Water-soluble EDC was recently known to be non-toxic and biocompatible, because it was not incorporated directly into the crosslinked sponge structure, but rather changed to water-soluble urea derivatives. The cytotoxicity of the urea derivative was found to be quite low compared with that of EDC [22]. In this paper, the addition of EDC changed the fiber diameter, water resistance, thermal behavior and mechanical properties, which was the result of the structural transition. But the reason of the structural transition was unclear. EDC conjugation resulted in the formation of a direct amide link within the silk fibroin. In our approach, the carboxylic groups on the silk fibroin were activated by EDC, and then the activated carboxylic groups were expected to react with amine groups. It had been reported that the blending of SF and chitosan also induced β-structure when the hydrogen bond forming between SF and chitosan [23]. Furthermore, Noishiki et al. reported that the β-structure formation of SF induced by contacting with cellulose whiskers when they prepared composite films of cellulose whisker and fibroin [24]. Here, we also found the structure transition from random coil to β-structure with the addition of EDC. It was interesting that the crosslinked as-spun SF nanofiber mats was water soluble which was the same as the non-crosslinked SF nanofiber mats, but the water resistance was greatly improved several days later. This seems to indicate the structural transition is a time-dependent process which needs a further investigation.

Table 3. Mechanical properties of SF nanofiber mats (1 – non-crosslinked SF mats; 2 – crosslinked SF mats)

Sample	Tensile strength, MPa	Elongation at break, %
1	7.9 ± 3.3	26.3 ± 8.2
2	8.6 ± 2.3	45.6 ± 15.8

CONCLUSIONS

In this study, we added EDC into the electrospin SF solution to prepare SF nanofiber mats with good water-resistance and mechanical properties. The results showed that the water-resistance, tensile strength and elongation at break were obviously improved due to the SF structural transition and EDC-crosslinke influence. The conformation transition of SF was approved by FTIR, X-ray diffraction and TG-DTA analysis. The SF nanofiber mats electrospun in this way had good water-resistance and mechanical property, which made it a promising candidate scaffold materials for tissue engineering.

ACKNOWLEDGMENTS

This work was supported by the National Natural Science Foundation Project of China (Nos. 30671041 and 30870642) and Natural Science Foundation and Natural College Science Foundation of Jiangsu Province (BK2009119, 06KJA18025).

REFERENCES

1. J. Perez-Rigueiro, C. Viney, J. Llorca, and M. Elices, Polymer **41**, 8433 (2000).
2. H. Y. Cheung and K. T. Lau, Key Eng. Mater. **326**, 457 (2006).
3. G. H. Altman, F. Diaz, C. Jakuba, T. Calabro, R. L. Horan, J. Chen, H. Lu, J. Richmond, and D. L. Kaplan, Biomaterials **24**, 401 (2003).
4. Y. Kawahara, K. Furukawa, and T. Yamamoto, Macromol. Mater. Eng. **291**, 458 (2006).
5. F. Zhang, B. Q. Zuo, H. X. Zhang, and L. Bai, Polymer **50**, 279 (2009).
6. S. J. He, R. Valluzzi, and S. P. Gido, Int. J. Biol. Macromol. **24**, 187 (1999).
7. Y. M. Yang, F. Ding, J. Wu, W. Hu, W. Liu, J. Liu, and X. S. Gu, Biomaterials **28**, 5526 (2007).
8. J. Magoshi, Y. Maghosi, and S. Nakamura, J. Polym. Sci. Polym. Phys. Edn. **19**, 185 (1981).
9. M. Tsukada, Y. Gotoh, M. Nagura, N. Minoura, N. Kasai, and G. Freddi, J. Polym. Sci. Part B, Polym. Phys. **32**, 961 (1994).
10. H. M. Powell, and S. T. Boyce, Biomaterials **27**, 5821 (2006).
11. Y. S. Choi, S. R. Hong, Y. M. Lee, K. W. Song, M. H. Park, and Y. S. Nam, J. Biomed. Mater. Res. **48**, 631 (1999).
12. V. Karageorgiou, L. Meinel, S. Hofmann, A. Malhotra, V. Volloch, and D. L. Kaplan, J. Biomed. Mater. Res. A **71**, 528 (2004).
13. J. S. Pieper, T. Hafmans, P. B. van Wachem, M. J. van Luyn, L. A. Brouwer, J. H. Veerkamp, and T. H. van Kuppevelt, J. Biomed. Mater. Res. **62**, 185 (2002).
14. Y. H. Shen, M. S. Shoichet, and M. Radisic, Acta Biomater. **4**, 477 (2008).
15. B. M. Min, L. Jeong, K. Y. Lee, and W. H. Park, Macromol. Biosci. **6**, 285 (2006).
16. D. M. Byler and H. Susi, Biopolymers **25**, 469 (1986).
17. M. Jackson and H. H. Mantsch, Crit. Rev. Biochem. Mol. Biol. **30**, 95 (1995).
18. C. X. Liang and K. Hirabayashi, Polymer **33**, 4388 (1992).
19. J. Magoshi, Y. Magoshi, S. Nakamura, N. Kasai, and M. Kakudo, J. Poly. Sci. Polym. Phys. Ed. **15**, 1675 (1977).
20. M. Tsukada, H. Shiozaki, Y. Goto, and G. Freddi, J. Appl. Polym. Sci. **50**, 1841 (1993).
21. B. M. Min, L. Jeong, K. Y. Lee, and W. H. Park, Macromol. Biosci. **6**, 285 (2006).
22. X. H. Wang, D. P. Li, W. J. Wang, Q.L. Feng, F. Z. Cui, Y. X. Xu, X. H. Song, and M. V. D. Werf, Biomaterials **24**, 3213 (2003).
23. X. Chen, W. Li, and T. Yu, J. Polym. Sci. Part B, Polym. Phys. **35**, 2293 (1997).
24. Y. Noishiki, Y. Nishiyama, M. Wada, S. Kuga, and J. Magoshi, J. Appl. Polym. Sci. **86**, 3425 (2002).